

Viologen Guest-Mediated Luminescence Emission Tuning and Photochromic Behavior by a Series of Viologen@Zn-MOF Materials

Haitao Han, Zheng Sun, Xia Zhao, Shujuan Yang, and Guannan Wang*

Cite This: <https://doi.org/10.1021/acsami.3c12012>

Read Online

ACCESS |



Metrics & More



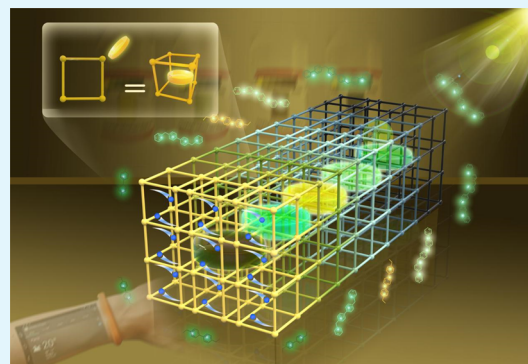
Article Recommendations



Supporting Information

ABSTRACT: The encapsulation of various guest molecules into the pores of metal–organic frameworks (MOFs) to form hybrid materials has attracted significant attention due to their unique spatial distribution and certain preferential geometry of the guests inside the MOFs. This arrangement often results in the guests exhibiting unique physical and chemical properties due to their intramolecular interactions with the host. In this article, five viologen derivatives were introduced as guests in a Zn-MOF with different benzene ring lengths, resulting in the formation of host–guest three-dimensional (3D) MOFs. The five compounds exhibited guest-dependent emission wavelength, color, and excellent photochromic behavior upon ultraviolet (UV) light radiation due to the distinct electronic transfer and $\pi\cdots\pi$ stacking interactions between the viologen guests and the host framework. This study provides a host–guest strategy for designing color-tunable luminescent and highly sensitive photochromic materials.

KEYWORDS: *host–guest, viologen-based MOFs, $\pi\cdots\pi$ stacking interactions, modulating emission, photochromic behavior*



1. INTRODUCTION

Electron transfer (ET) smart materials, such as tunable luminescent and photochromic materials based on a host–guest platform, have attracted significant attention due to their potential applications in light sensing, detectors, information storage, anticounterfeiting, and others.^{1–3} Various host–guest platforms have been documented through well-developed design and synthesis technology.^{4–6} The luminescent and photochromic properties of the materials depend on their components and the interactions between hosts and guests. Consequently, researchers can exercise significant control over these and other chemical and physical properties. Therefore, selecting hosts and guests and designing an ideal host–guest platform are key to controlling the physical and chemical properties of the materials.

Metal–organic frameworks (MOFs) are well-developed crystalline porous materials self-assembled from inorganic nodes and organic ligands. They have been extensively used in catalysis, chemical sensing, biomedicine, and other fields owing to their significant chemical stability and high surface areas.^{7–9} Moreover, the crystalline structures, pore sizes, and functionality of MOFs can be modulated at the molecular level by choosing the appropriate organic components, making them promising candidates as donors. Further, viologen derivatives, as cationic electron-deficient organic ligands, can react sensitively and rapidly to various external stimuli accompanied by a wealth of coloration phenomena. Previously, different smart materials have been constructed using viologen

derivatives.^{10–12} Hence, it is a logical choice to construct ET smart materials with MOFs as hosts and viologen ligands as guests.^{13–16}

Previous studies have demonstrated that loading different functional guest molecules into MOFs results in tunable emission colors via intermolecular interactions between the guest molecules and the MOF skeleton. This tunable color property has been used in sensing and luminophore applications.^{17–19} For example, Bu et al. loaded a series of electron-rich aromatic guests into an electron-deficient MOF, realizing charge-transfer-based emission color changes.²⁰ Li et al. presented a new strategy to encapsulate multiple dyes into nanocrystalline ZIF-8 pores. Using this strategy, they achieved a finely tuned white emission color by varying the components and concentrations of encapsulated dyes.²¹

These reports demonstrate that viologens present in the pores of MOFs can significantly impact emissions from electronic interactions between viologens and the framework. However, reports of viologen guest molecules modulating the emission color are rare. Furthermore, the photoluminescence (PL) modulations of some ET smart materials are limited to

Received: August 13, 2023

Revised: October 10, 2023

Accepted: October 11, 2023

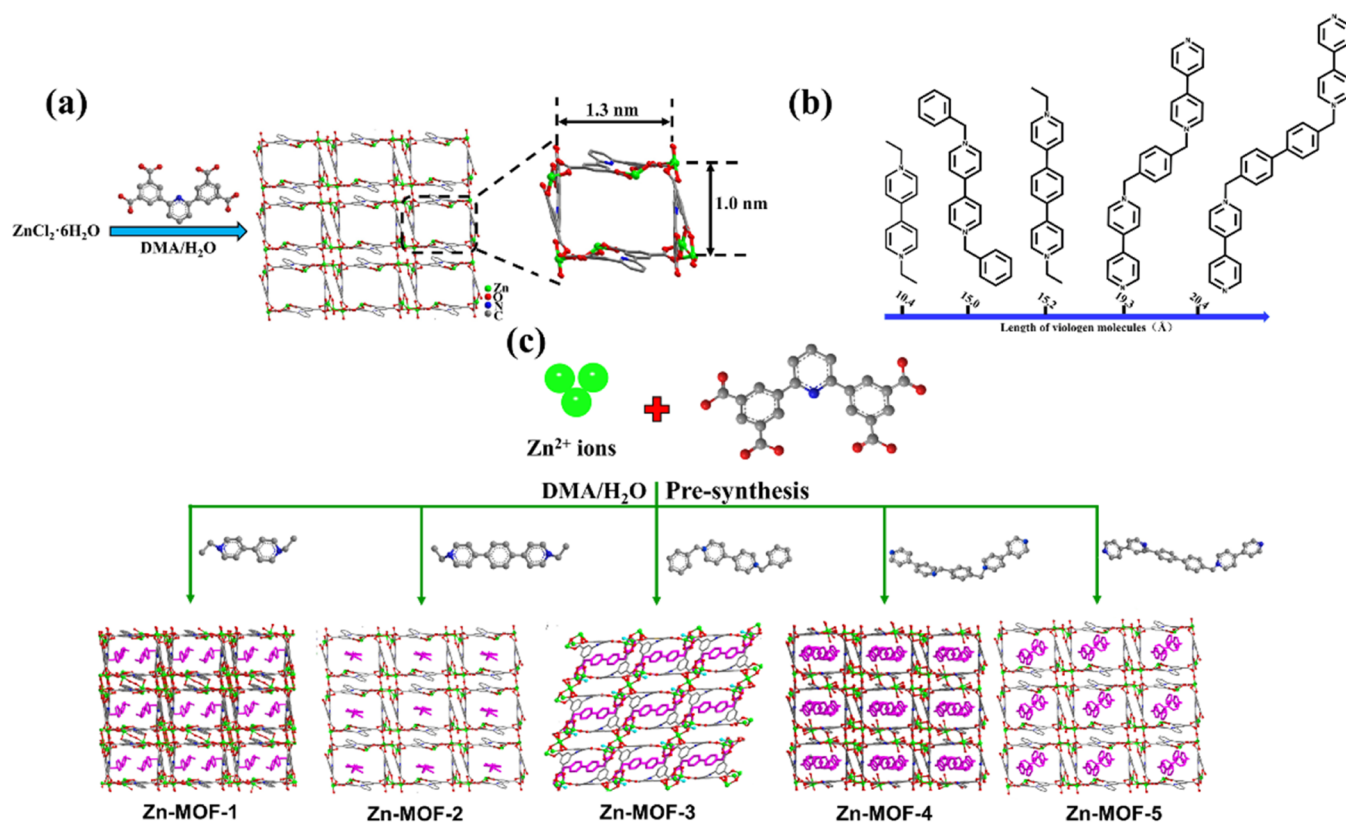


Figure 1. (a) Preparation of Zn-MOF-0. The coordinate DMA molecules are omitted for clarity. (b) Five viologen molecules used in this study (arranged by length). (c) Encapsulation of guest molecules forming host–guest materials.

simple on/off switching with coloring/bleaching behaviors, with no change in the emitted colors.^{22–24} Most viologen-based MOFs are reported to be sensitive to ultraviolet (UV) light. They can detect sunlight with a minimum detection intensity of $1 \mu\text{W}/\text{cm}^2$ (Table S1).^{25,26} Natural and room light detection by the viologen-based MOFs are rarely reported due to the high detection limit toward UV light. In addition, the reported sensors for UV light decolor to the original color expanding several tens of hours or even several days, restricting their convenience and portability in daily life (Table S2).^{22–26}

Herein, a three-dimensional (3D) Zn-MOF containing well-defined two-dimensional (2D) channels was utilized as a host framework. Five viologen molecular derivatives served as guest molecules, forming host–guest materials. Consequently, these five host–guest materials, named Zn-MOFs-1–5 based on viologen molecules, revealed highly tunable guest-dependent emissions from green to yellow and excellent photochromic properties. Further, Zn-MOF-3 detected natural and room light with a minimum detection intensity of $0.1 \mu\text{W}/\text{cm}^2$, successfully developed in photosensitive reagents' warning labels. Zn-MOF-1 showed fast recovery from the color saturation state to the initial color state toward UV light and could be used as a portable UV-sensitive card for UV light detection.

2. EXPERIMENTAL SECTION

2.1. Synthesis of Zn-MOFs-0–5. **2.1.1.** $[\text{Zn}_4(\text{pdda})_2(\text{H-DMA})(\text{H}_2\text{O})_2(\text{OH})]\cdot[\text{DMA}]_5$ (**Zn-MOF-0**). Colorless single crystal blocks of Zn-MOF-0 were obtained by the solvothermal reaction of the mixture of $\text{ZnCl}_2\cdot 6\text{H}_2\text{O}$ (0.05 g, 0.1 mmol), 5,5'-(pyridine-3,5-diyl)-diisophthalic acid (0.025 g, 0.06 mmol, H_4pdda), *N,N*-dimethylacetamide (DMA) (2.0 mL), and water (3.0 mL) in a 15 mL Teflon-

lined autoclave which was heated to $130 \text{ }^\circ\text{C}$ for 3 days. Subsequently, the autoclave was slowly cooled to $20 \text{ }^\circ\text{C}$ at $4 \text{ }^\circ\text{C}\cdot\text{h}^{-1}$. The crystals were collected by filtration. Yield: 36% based on H_4pdda . Elemental analysis: calcd (%) for $[\text{Zn}_4\text{O}_{25}\text{N}_8\text{C}_{66}\text{H}_{79}]$ (including disordered solvent molecules): C 48.19, H 4.74, and N 6.81; found: C 49.26, H 4.25, and N 6.53. FT-IR (cm^{-1}) (Figure S1): 3388(w), 1618(s), 1572(s), 1432(m), 1403(m), 1355(s), 1317(w), 1274(s), 1182(w), 1112(w), 1079(w), 1091(w), 928(m), 806(m), 776(s), 728(s), 657(s), and 632(w).

2.1.2. $[\text{Zn}_8(\text{pdda})_4(\text{DMA})(\text{H}_2\text{O})_7(\text{OH})_2]^{2-}\cdot[\text{debpy}]^{2+}\cdot[\text{DMA}]_{10}$ (**Zn-MOF-1**). Light yellow single crystal blocks of Zn-MOF-1 were obtained by the solvothermal reaction of the mixture of $\text{ZnCl}_2\cdot 6\text{H}_2\text{O}$ (0.05 g, 0.1 mmol), H_4pdda (0.025 g, 0.06 mmol), 1,1'-diethyl-[4,4'-bipyridine]-1,1'-dium.dibromide ($\text{debpy}\cdot\text{Br}_2$, 0.02 g, 0.05 mmol), *N,N*-dimethylacetamide (DMA) (2.0 mL), and water (3.0 mL) in a 15 mL Teflon-lined autoclave which was heated to $110 \text{ }^\circ\text{C}$ for 1 day. Subsequently, the autoclave was slowly cooled to $20 \text{ }^\circ\text{C}$ at $4 \text{ }^\circ\text{C}\cdot\text{h}^{-1}$. The crystals were isolated by filtration, which were washed with DMA and then dried in air. Yield: 19% based on $\text{debpy}\cdot\text{Br}_2$. Elemental analysis: calcd (%) for $[\text{Zn}_8\text{O}_{51}\text{N}_{17}\text{C}_{142}\text{H}_{169}]$ (including disordered solvent molecules): C 49.39, H 4.90, and N 6.90; found: C 49.85, H 4.25, and N 6.62. FT-IR (cm^{-1}) (Figure S2): 3371(w), 1615(s), 1571(s), 1396(s), 1353(s), 1271(s), 1181(m), 1080(m), 1012(m), 924(m), 820(m), 772(s), 725(s), 651(s), and 564(m).

2.1.3. Zn-MOF-2. Yellow single crystal strips of Zn-MOF-2 were obtained by the solvothermal reaction of the mixture of $\text{ZnCl}_2\cdot 6\text{H}_2\text{O}$ (0.05 g, 0.1 mmol), H_4pdda (0.025 g, 0.06 mmol), $150 \mu\text{L}$ of a H_2O solution of 4,4'-(1,4-phenylene)bis(1-ethylpyridin-1-ium)-dibromide (0.1 g/mL, $\text{pbepy}\cdot\text{Br}_2$), *N,N*-dimethylacetamide (DMA) (2.0 mL), and water (3.0 mL) in a 15 mL Teflon-lined autoclave which was heated to $110 \text{ }^\circ\text{C}$ for 1 day. Subsequently, the autoclave was slowly cooled to $20 \text{ }^\circ\text{C}$ at $4 \text{ }^\circ\text{C}\cdot\text{h}^{-1}$. The crystals were isolated by filtration, which were washed with DMA and then dried in air. Yield: 16% based on $\text{pbepy}\cdot\text{Br}_2$. FT-IR (cm^{-1}) (Figure S3): 3381(w), 3219(w), 1615(s), 1571(s), 1430(m), 1403(m), 1356(s), 1275(s), 1184(m),

1110(m), 1019(m), 924(m), 803(s), 776(s), 725(s), 655(s), and 567(m).

2.1.4. $[Zn_5Cl_2(pdda)_2(OH)_2]^{2-} \cdot [dbbpy]^{2+} \cdot [DMA]_5$ (Zn-MOF-3). Yellow single crystal blocks of Zn-MOF-3 were obtained under the same reaction conditions as those for Zn-MOF-1, except for replacing debpy-Br₂ with 1,1'-dibenzyl-[4,4'-bipyridine]-1,1'-diium-dichloride (dbbpy-Cl₂) (0.01 g, 0.02 mmol). The crystals were isolated by filtration, which were washed with DMA and then dried in air. Yield: ca. 23% based on dbbpy-Cl₂. Elemental analysis: calcd (%) for Zn₅Cl₂O₂₃N₉C₈₆H₈₅ (including disordered solvent molecules): C 51.39, H 4.23, and N 6.27; found: C 51.64, H 4.04, and N 6.37. FT-IR (cm⁻¹) (Figure S4): 3523(w), 3293(m), 3055(m), 1618(s), 1568(s), 1430(m), 1406(m), 1362(s), 1353(s), 1275(m), 1072(m), 921(m), 823(m), 820(m), 776(s), 739(s), 655(s), and 564(m).

2.1.5. $[Zn_8(pdda)_4(H_2O)_8(OH)_2]^{2-} \cdot [pbbpy]^{2+} \cdot [DMA]_6$ (Zn-MOF-4). Flat-shaped yellow single crystals of Zn-MOF-4 were obtained under the same reaction conditions as Zn-MOF-0, except for adding 1,1'-(1,4-phenylenebis(methylene))bis((4,4'-bipyridin)-1-ium)-dichloride (pbbpy-Cl₂) (0.01 g, 0.02 mmol). The crystals were isolated by filtration, which were washed with DMA and then dried in air. Yield: ca. 14% based on pbbpy-Cl₂. Elemental analysis: calcd (%) for [Zn₈O₄₈N₁₂C₁₃₆H₁₂₈] (including disordered solvent molecules): C 50.72, H 3.97, and N 5.22; found: C 50.09, H 3.85, and N 5.16. FT-IR (cm⁻¹) (Figure S5): 3208(w), 3058(m), 1615(s), 1571(s), 1430(m), 1400(m), 1359(s), 1353(s), 1268(m), 1072(m), 924(m), 776(s), 725(s), 655(s), and 567(m).

2.1.6. Zn-MOF-5. Flat-shaped yellow single crystals of Zn-MOF-5 were obtained under the same reaction conditions as Zn-MOF-0 except for adding 1,1'-(1,1'-biphenyl)-4,4'-diylbis(methylene))bis((4,4'-bipyridin)-1-ium)-dichloride (bdbpy-Cl₂) (0.01 g, 0.02 mmol). The crystals were collected by filtration. Yield: 13% based on bdbpy-Cl₂. FT-IR (cm⁻¹) (Figure S6): 3267(w), 3055(w), 1622(s), 1568(s), 1575(w), 1430(m), 1392(m), 1353(m), 1271(m), 1171(w), 1103(m), 1005(m), 921(m), 719(s), 651(s), 625(m), and 560(m).

2.2. UV Doses Detection Procedures. For the UV-dependent coloration measurements, a 15 W light lamp (365 nm UV type, PhilipsHolland) was used as the irradiation source. The UV light intensity was measured by a UV-A photometer (Beijing Shida Optoelectronics Technology Co., Ltd.) and controlled with the distance between the lamp and crystals sample. In order to simulate sunlight, the irradiation sources were used by UVA and UVB lamps (UVA20WT12-600320-400 nm and UVB20WT12-600 280-320 nm LONGPRO China) measured by a 340A UV light meter (Lutron, America).

2.3. H₂O₂ Decomposition Rate Measurement Procedures under Different Times. In order to measure unknown H₂O₂ concentrations under different times, we used UV-visible (UV-vis) absorption spectra of the TMB-derived oxidation product in the presence of the ZnMnFe₂O₄ nanomaterial as a catalyst under 30, 20, and 15% wt of H₂O₂ at room temperature.²⁷ Afterward, standard curves are plotted based on the relationship between maximum values of the TMB-derived oxidation product absorbance and concentrations of H₂O₂. In the end, the unknown H₂O₂ concentrations are determined at different times based on standard curves.

3. RESULTS AND DISCUSSION

3.1. Synthesis and Molecular Structures. ZnCl₂·6H₂O and H₄pdda were reacted in a mixture of dimethylacetamide (DMA) and water (H₂O) under solvothermal conditions that provided flat-shaped colorless crystals of Zn-MOF-0 (Figure 1a). Zn-MOF-0 consists of a 2D square channel with an approximate diameter of 1.3 nm × 1.0 nm, which is suitable for encapsulating viologen molecular derivatives with proper dimensions. As a result, five hybrid materials Zn-MOFs-1-5 were successfully obtained by introducing five viologen molecules of varying lengths between 10.4 and 20.4 Å into the reaction system through a self-assembly mode (Figure 1b,c). The successful fabrication of five crystalline materials

demonstrates that the inclusion of guest molecules does not interfere with the relatively stable coordination-directed assembly inherent in Zn-MOF-0. In addition, we also attempted a postsynthesis method to prepare viologen-based host-guest compounds, but we could not obtain them due to DMA solvent molecules occupying the pores of Zn-MOF-0, which prevents the entry of viologen derivatives. Single-crystal diffraction experiments revealed that compound Zn-MOF-0 crystallizes in the triclinic space group with the space group *P*-1. As shown in Figure S7, the asymmetric unit is constituted by four crystallographically independent Zn²⁺ ions and two pdda⁴⁻ ligands. The Zn1 site shows tetrahedral geometry with one OH⁻ and three O atoms from three different pdda⁴⁻ ligands. Zn2 and Zn3 are both five-coordinated, but their coordination environments are different: Zn2 is coordinated by one OH⁻, one H₂O molecule, and three O atoms from three different pdda⁴⁻ ligands; Zn3 is coordinated by one OH⁻ and three O atoms from three different pdda⁴⁻ ligands. Zn4 is four-coordinated by one H₂O molecule, one O atom from a coordinated DMA molecule, and two O atoms from two different pdda⁴⁻ ligands. The carboxyl O atoms from the pdda⁴⁻ ligands have monodentate and bidentate coordination modes and each Zn²⁺ ion connects two pdda⁴⁻ ligands to form a 3D framework (Figure S8). Zn-MOF-1 crystallizes in the triclinic space group *P*-1. Zn-MOF-1 contains square channels with a pore size of 1.2 nm × 1.1 nm with the debpy²⁺ guest immobilized in the channels and produces a nonporous host-guest architecture (Figure S9a). As shown in Figure S9b, the asymmetric unit of Zn-MOF-1 possesses one debpy²⁺ guest molecule, eight crystallographic Zn²⁺ ions, and four pdda⁴⁻ ligands. Zn1 is five-coordinated by one OH⁻, one H₂O molecule, and three O atoms from three different pdda⁴⁻ ligands. Zn2 is also five-coordinated by one OH⁻, two H₂O molecules, and two O atoms from two different pdda⁴⁻ ligands. Zn3 is four-coordinated by one OH⁻, one H₂O molecule, and two O atoms from two different pdda⁴⁻ ligands. Zn4 is six-coordinated by one OH⁻, two H₂O molecules, and three O atoms from three different pdda⁴⁻ ligands. Zn5 is five-coordinated by one OH⁻ and four O atoms from three different pdda⁴⁻ ligands. Zn6 is four-coordinated by one OH⁻ and three O atoms from three different pdda⁴⁻ ligands. Zn7 is six-coordinated by three H₂O molecules and three O atoms from two different pdda⁴⁻ ligands. Zn8 is five-coordinated by one H₂O molecule, one O atom from the coordinated DMA molecule, and three O atoms from two pdda⁴⁻ ligands. The carboxyl O atoms from four pdda⁴⁻ ligands have two different coordination modes. The first is the coordination mode in case, that is, both carboxylic acid oxygen atoms from pdda⁴⁻ are involved in coordination and are coordinated to two different Zn²⁺ ions. Another mode is only where one O atom from pdda⁴⁻ is coordinated by one Zn²⁺ ion (Figure S10). Neighboring pdda⁴⁻ ligands link Zn²⁺ ions to form a 3D supramolecular framework. Zn-MOF-3 crystallizes in the monoclinic system with the space group *C*2/*c*. Zn-MOF-3 has one-dimensional (1D) channels and guest molecules accommodated in channels which possess rhomboid pores of 0.8 nm × 0.7 nm (Figure S11a). In an asymmetrical unit, there are three crystallographic Zn²⁺ ions, one pdda⁴⁻ ligand, and half of the dbbpy²⁺ cation (Figure S11b). Zn1 is six-coordinated through two OH⁻ and four O atoms from two different pdda⁴⁻ ligands, displaying a distorted octahedral geometry. Zn2 is four-coordinated by one OH⁻ and three O atoms from three pdda⁴⁻ ligands. Zn3 exhibits tetrahedral

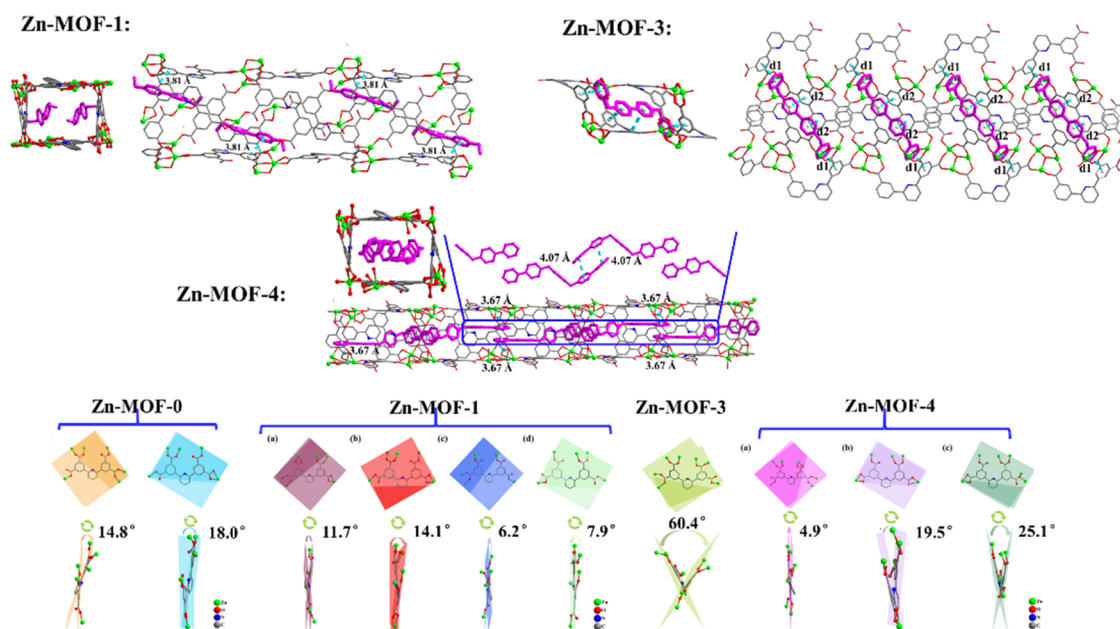


Figure 2. Top: the channel of Zn-MOFs occupied by guests and the $\pi\cdots\pi$ stacking interactions between guests and the host structure in Zn-MOFs. d_1 : 3.58 Å and d_2 : 3.65 Å. Bottom: the dihedral angles between the H₄pdda ligand and ligand planes in Zn-MOFs.

geometry with one Cl⁻, one OH⁻, and two atoms from two different pdda⁴⁻ ligands. The carboxyl O atoms from pdda⁴⁻ ligands also have two coordinate modes and each pdda⁴⁻ ligand connects with seven Zn²⁺ ions, forming a nonporous 3D host–guest complex. Zn-MOF-4 has an identical space group with *P*-1, as shown in Figure S13a. The distorted guests pbbpy²⁺ occupy one-dimensional channels with the diameters being 1.2 nm × 1.0 nm. As shown in Figure S13b, the asymmetric unit is constituted by eight crystallographically independent Zn²⁺ ions, four pdda⁴⁻ ligands, and one pbbpy²⁺ guest. Zn1 and Zn2 are four-coordinated by one OH⁻ and three O atoms from pdda⁴⁻ ligands. Zn3 is five-coordinated by one OH⁻, one H₂O molecule, and three O atoms from pdda⁴⁻ ligands. Zn4 is five-coordinated by one OH⁻, three H₂O molecules, and one O atom from one pdda⁴⁻ ligand. Zn5 is five-coordinated by one OH⁻, two H₂O molecules, and two O atoms from two pdda⁴⁻ ligands. Zn6 is also five-coordinated by one OH⁻ and four O atoms from three pdda⁴⁻ ligands. Zn7 and Zn8 are six-coordinated by three H₂O molecules and three O atoms from two pdda⁴⁻ ligands. The carboxyl O atoms from pdda⁴⁻ ligands adopt three coordinate modes with Zn²⁺ ions, forming a nonporous three-dimensional host–guest complex (Figure S14). Furthermore, through careful observation of the structures of Zn-MOFs-1, 3, and 4, we discovered that the arrangement of the guest molecules in the MOFs was variable. In Zn-MOFs-1 and 4, the guest molecules filled the pores uniformly (Figure 2), although their arrangement within the pores of Zn-MOFs-1 and 4 was slightly different. In Zn-MOF-1, there was a distinct angle formed between the guest molecules and the host structure. Conversely, in Zn-MOF-4, the guest molecules situated themselves parallel to the channels, occupying rectangular cavities within the 3D framework (Figure 2). Notably, in Zn-MOF-3, the guest molecules partially filled the one-dimensional channels in a direction perpendicular to the channels and were parallel to each other. In addition, the X-ray diffraction data also suggested that intermolecular forces existed between the guest molecules and the host structures in Zn-MOFs-1, 3,

and 4. The $\pi\cdots\pi$ interactions between the guests and H₄pdda ligands were 3.81 Å in Zn-MOF-1, 3.58 and 3.65 Å in Zn-MOF-3, and 3.67 Å in Zn-MOF-4 (Figure 2). The close stacking of viologens and H₄pdda ligands indicates relatively strong interactions between them, which could facilitate donor–acceptor interactions. Besides, compared with the structures of Zn-MOFs-0, 1, and 4, the structure of Zn-MOF-3 has changed slightly. Therefore, we explored the degree of distortion of the H₄pdda ligands in these compounds. The degree of distortion of the benzene ring of H₄pdda ligands in Zn-MOFs-1 and 4 is slight and the dihedral angle between the H₄pdda ligand and ligand planes is similar to that of Zn-MOF-0, yet the dihedral angle of Zn-MOF-3 between the H₄pdda ligand and ligand planes through the benzene ring is 59.5°, which results in slightly different structures compared to Zn-MOF-0. These results also indicate that strong $\pi\cdots\pi$ stacking interactions (3.58 and 3.65 Å) between the viologen guest and H₄pdda ligand play an important role in forming molecular crystals of Zn-MOF-3. However, the single-crystal X-ray diffraction structures of Zn-MOFs-2 and 5 could not be obtained, may be due to the guests' irregular arrangement within the crystal lattices and low occupancy, resulting in a low scattering intensity of X-rays by the guest molecules. Therefore, their structures were confirmed by powder X-ray diffraction, appearance color, fluorescence, and thermogravimetric analysis (TGA). The phase purity of bulk samples of Zn-MOFs-0–5 was confirmed by powder X-ray diffraction (PXRD) (Figures S15–S20). TG analysis reveals that all compounds have similar TG behaviors (Figure S21); that is, five compounds showed a slow weight loss with the release of the lattice solvent molecules until 360 °C and then a steep weight loss due to the decomposition of the compound. The similar TG behaviors would be due to their similar structures, expect of the guest molecules. Additionally, Zn-MOFs-1–5 showed a slower weight loss than that of Zn-MOF-0 due to the inclusion of viologen molecules in Zn-MOFs-1–5.

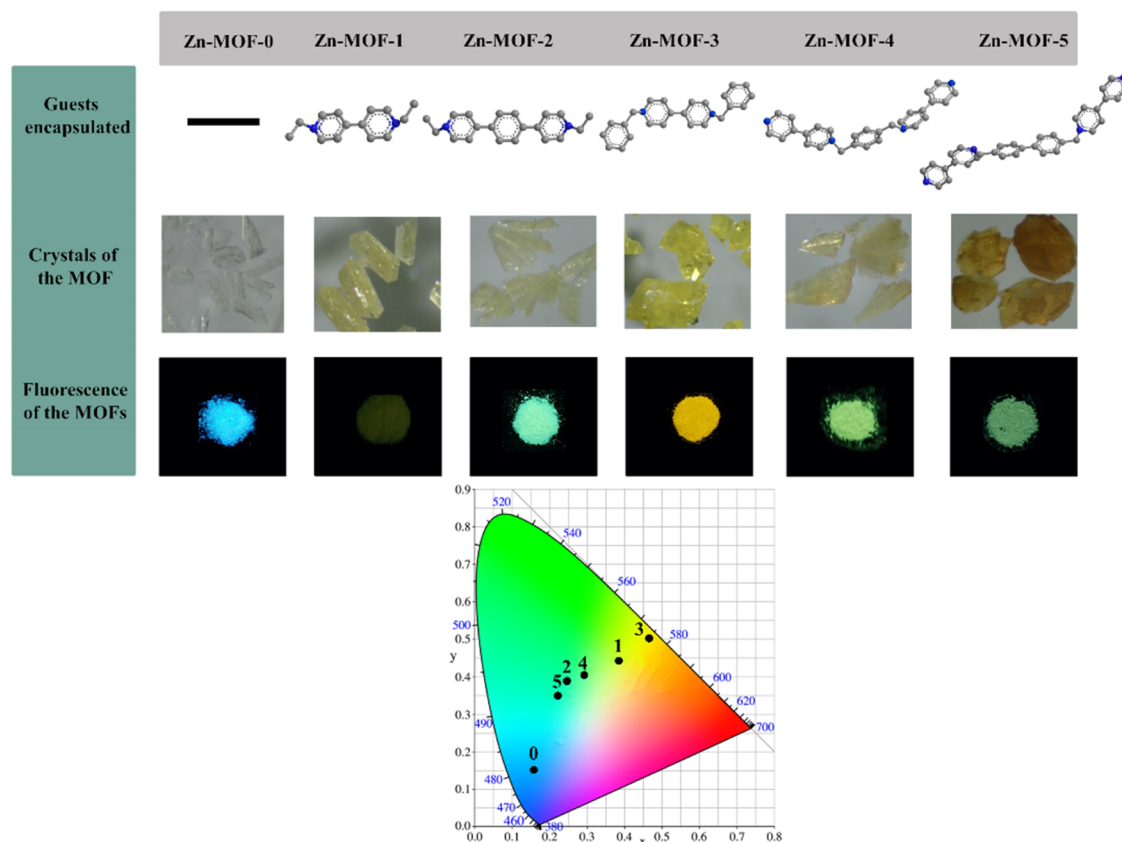


Figure 3. Guest-dependent optical (top) and luminescent (middle) images of crystals and the CIE color coordinates of the Zn-MOFs (bottom).

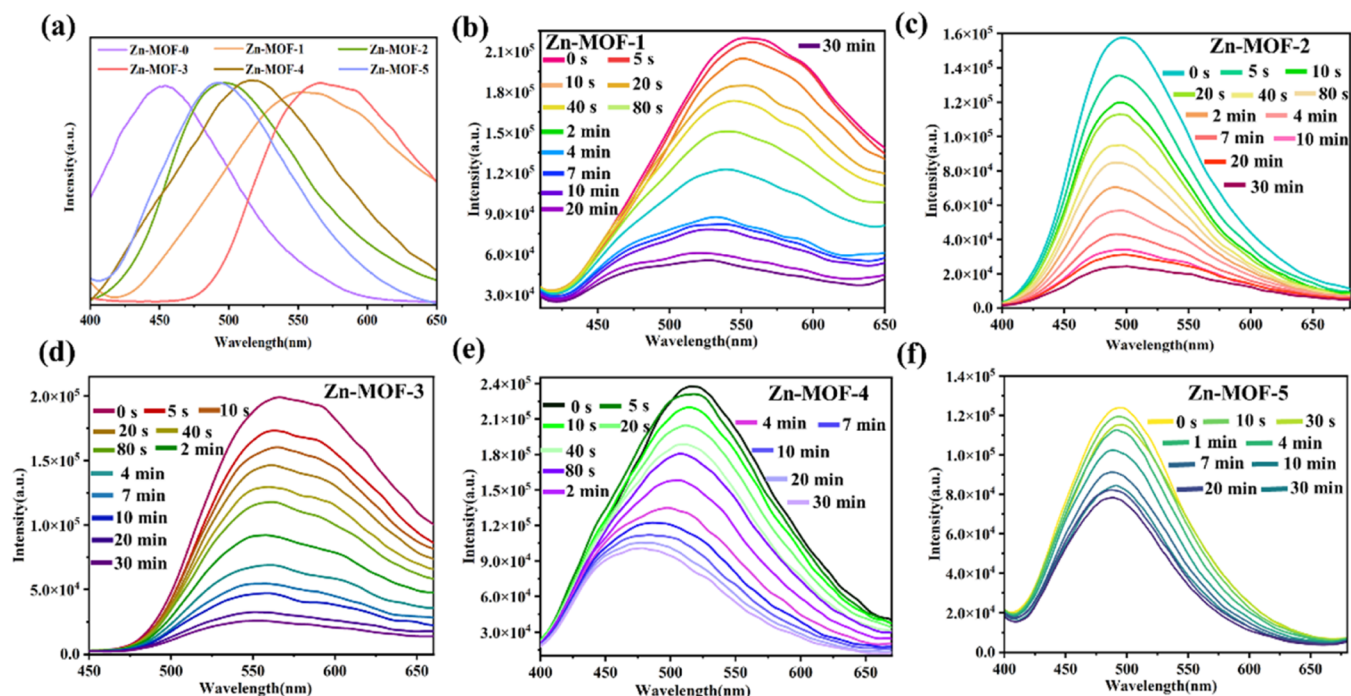


Figure 4. (a) Solid-state photoluminescence (PL) spectra of Zn-MOFs-0-5 ($\lambda_{\text{ex}} = 365$ nm for Zn-MOFs-1-5 and $\lambda_{\text{ex}} = 364$ nm for Zn-MOF-0). (b-f): PL spectral changes after irradiation with 365 nm UV light (0.5 mW/cm^2 for Zn-MOFs-1, 3, 4, and 5 and 2.5 mW/cm^2 for Zn-MOF-2) at different times.

3.2. Fluorescent Properties. Viologen-based compounds have been reported to exhibit special luminescence emissions originating from the charge transfer between the framework

and viologen molecules.²⁸⁻³⁰ Thus, their luminescent properties were first investigated. Notably, Zn-MOFs-1-5 showed guest-dependent luminescence compared with Zn-MOF-0

(Figure 3). The corresponding CIE coordinates of their emissions were calculated; the values spanned a wide range from green to yellow (Figure 3). As shown in Figure 4a, Zn-MOF-0 emitted at 454 nm when excited with a 364 nm laser. The emissions of Zn-MOFs-1–5 (496–565 nm) were red-shifted compared with Zn-MOF-0, and the extent of the red shift depended on the encapsulated guests, which may be ascribed to the charge transfer between guest viologen molecules and the host framework. The average lifetime (τ_{av}) of Zn-MOF-0 was 4.75 ns, and the average lifetimes of Zn-MOFs-1–5 were in the range of 1.4–37.69 ns (Figure S22; Table S4, Supporting Information). The photoluminescence quantum yield (PLQY) (%) of Zn-MOF-0 was 12.9%, while that of the other MOFs was 2.2–22.7%. These results indicate that a typical charge-transfer interaction occurs between viologen guests and the host framework. Moreover, the broad emission range of the five hybrid materials suggests that fluorescence emission modulation can be achieved by using the MOF as a host and different viologen molecules as guests. Additionally, Zn-MOFs-1–5 simultaneously exhibited luminescence quenching phenomenon and photochromic transition with PL color evolution upon continuous 365 nm UV irradiation (Figure 4b–4f). Under continuous 365 nm UV irradiation, the emission intensities of the Zn-MOFs-1, 3, 4, and 5 drastically decreased to 73.0, 86.8, 57.6, and 36.8% of the original intensity, respectively, upon 900 mJ/cm² irradiation (0.5 mw/cm², 30 min). Meanwhile, Zn-MOF-2 is less sensitive toward UV light than the other Zn-MOFs. The emission intensity of Zn-MOF-2 decreased to 85.2% of the original intensity upon 4.5 J/cm² irradiation (2.5 mw/cm², 30 min). Therefore, among the five hybrid materials, Zn-MOF-3 has the highest quenching efficiency, which is attributed to the rapid charge-transfer ability between the MOF host and the viologen guest. Besides, compared with Zn-MOF-0, Zn-MOFs-1, 3, 4, and 5 were blue-shifted by 24, 14, 38, and 6 nm, respectively; Zn-MOF-2 was red-shifted by 3 nm (See Figure S23; Table S5, Supporting Information). The changes mentioned above can also be visualized by the gradual transition of the emission color from pinkish green to pine forest green for Zn-MOF-2, patina to light green-gray for Zn-MOF-4, and stone green to blue for Zn-MOF-5, resulting in photomodulated luminescence (Figure 5a). Wavelength shifts of 38 nm for Zn-MOF-4 upon exposure to external stimuli are rarely reported for viologen-based MOFs. Consequently, these materials could be potentially applied in photomodulated color switching by an easy UV light irradiation mode.

3.3. Photochromism. The photochromism of Zn-MOFs-1–5 was examined in air at room temperature since viologen-based compounds possess excellent photochromic properties. Under continuous UV light exposure, Zn-MOFs-1–5 showed evident color changes (Figure 5b). After 60 min of UV irradiation, the color of Zn-MOFs-1–5 reached saturation and then turned gray, brown, dark green, dark blue, and light blue, respectively. The five MOFs showed different photochromic abilities. Among all of the MOFs, Zn-MOF-3 produced the best photochromic abilities. After 10 s of UV irradiation at a low intensity of 0.5 mw/cm², a clear color change from yellow to cyan blue was observed. A response was observed with a UV irradiance intensity as low as 0.1 μ W/cm² (Figure S24), which is comparable to commercialized UV light radiation devices, lower than that reported for ultraviolet light detection materials.^{25,26,31–34} The color-saturated samples of Zn-MOFs-1–5 were completely decolorized after being kept in

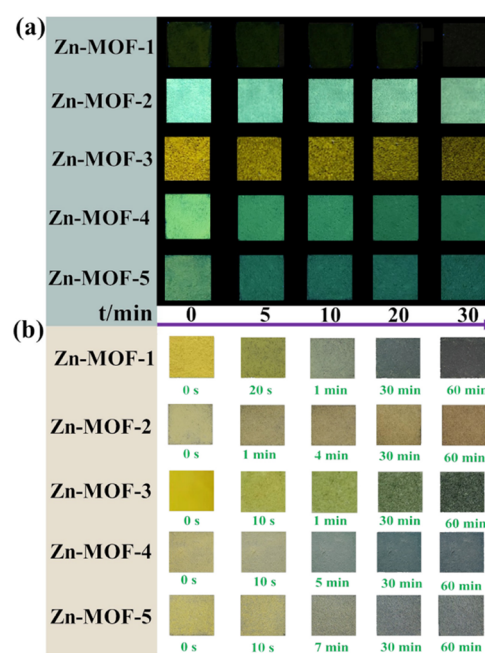


Figure 5. (a) Photomodulated luminescence over time under 365 nm light exposure. Zn-MOFs-1–5 were loaded on a quartz slide with a dimension of 1.5×1.5 cm². (b) Photochromism of Zn-MOFs-1–5 upon 365 nm UV irradiation over different times.

the dark for 9, 28, 41, 25, and 47 h at room temperature, respectively (Figure S25). This reversible color conversion could be repeated three times without a significant color loss.

3.4. Application in Direct Readout UV Colorimetric Dosimeters. Photosensitive reagents are photolyzed under natural or sunlight irradiation. However, protective photo-sensitive colorimetric dosimeters toward these reagents are rarely documented due to the requirement of low light detection limits. Zn-MOF-3 displays fast and sensitive responses toward low doses of natural and room light (Figures S26–S27). This property is suitable for applications as a photosensitive colorimetric dosimeter for photosensitive reagents. To explore the practical applications of Zn-MOF-3, a color matching chart was prepared with 30 mg of Zn-MOF-3 on a silicone board (2×2 cm²). A color matching chart was prepared by exposing samples to natural light at different times and used as a reference for an unknown concentration of H₂O₂ (Figures S28–S31). Then, the matching chart was attached to the top of a H₂O₂ reagent bottle and exposed to natural light for varying time periods. As shown in Figure 6a, when a H₂O₂ reagent bottle is exposed to natural light for 0.5, 4, and 9 h, respectively, the concentration of H₂O₂ decreases from 30 wt % to 29.7, 26.6, and 19.1%, accompanied by a color change from yellow to light green, green, and dark green in the matching chart. The low limit of the H₂O₂ decomposition rate was 0.3%. Meanwhile, the changed color of the matching chart remained unchanged for at least 24 h when kept in the dark. These results indicated that Zn-MOF-3 could be utilized as a warning label for the decomposition rate of H₂O₂ in natural light. Due to the fast recovery from the color saturation state to the initial color state toward UV light for Zn-MOF-1, we developed a portable UV colorimetric dosimeter. As is well known, ultraviolet (UV) rays in the sunlight are primarily responsible for skin damage and are categorized into UVA (400–320 nm), UVB (315–280 nm), and UVC (290–100

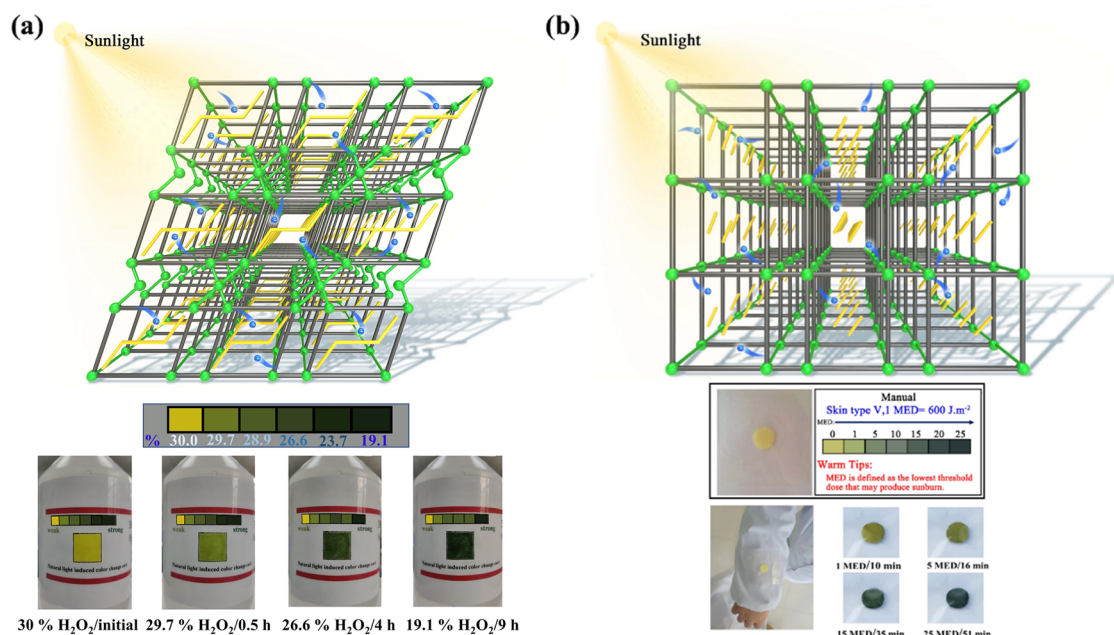


Figure 6. (a) Zn-MOF-3 as a photosensitive colorimetric dosimeter for the H₂O₂ decomposition rate under natural light (Feb 25, 2023, in Jining, China). (b) Zn-MOF-1 made as a UV-sensitive card by MED (Feb 24, 2023, in Jining, China).

nm) rays; the ozone layer completely filters UVC. A UV colorimetric dosimeter alerts users against excessive solar UVA–UVB exposure and can operate in the range of the minimal erythemal dose (MED). MED is the minimum amount of UVR likely to cause erythema for most Asians, i.e., with skin type V (600 J/m²).^{35,36} Based on this, a sunlight colorimetric dosimeter was developed to determine personal UVA and UVB radiation doses in real time (Figure 6b). As shown in Figure 6b, 20 mg of samples were loaded in a thin film as a colorimetric dosimeter, and the film was attached on the surface of the user's clothing. Similarly, a color matching chart was also prepared by exposing samples to UVA and UVB at different MEDs and used as a reference for an unknown MED (Figure S32). From the color changes of the colorimetric dosimeter on the user's clothing, the user can obtain information about sunlight radiation doses. Further, the dosimeter can decolor to the original color when kept in the dark for 5 h or heated at 50 °C for 30 min, making it suitable for practical applications.

3.5. Mechanism of Photochromism and Photoluminescence Modulation. The powder X-ray diffraction (PXRD) patterns observed in both the preirradiation and postirradiation samples closely matched those of the originally synthesized sample (Figures S33–S37). Similarly, the IR spectra of complexes Zn-MOFs-1–5 before and after exposure to UV–vis light showed a high degree of overlap (Figures S38–S42). These results suggest that the observed photochromism was not a result of structural alterations or photolysis. The UV–vis diffuse reflectance and electron spin resonance (ESR) spectra of the Zn-MOFs were recorded before and after UV light treatment to explore the mechanism of their photochromic behaviors. Upon UV light irradiation, the UV–vis spectra showed new strong bands centered at 627–751 nm (Figures S43–S47), while the ESR spectra showed stronger and symmetric single-peak radical signals, confirming the existence of photogenerated radicals (Figures S48–S52).^{31–34,37,38} For Zn-MOFs-1, 3, and 4, the shortest

distances between the O of carboxylate groups and the N of the pyridinium unit were 3.48, 3.83, and 3.56 Å, respectively, satisfying the photoinduced electron paths. The shorter distances are more favorable for electron transfer. Additionally, as previously reported, the small dihedral angles between the two pyridinium rings were more conducive to the photoinduced reduction of viologens and the stability of free radicals.^{39,40} Zn-MOF-3 showed the smallest dihedral angle (the dihedral angles between the two pyridinium rings for Zn-MOFs-1, 2, and 3 are 29.4, 0, and 11.95°, respectively) and showed the strongest $\pi\cdots\pi$ stacking interactions. The small dihedral angle and strong $\pi\cdots\pi$ stacking interactions between the bipyridinium ring and H₄pdda ligand lead to fast photochromism of Zn-MOF-3 in the presence of UV light. X-ray photoelectron spectroscopy (XPS) spectra were collected to further explore the photochromic mechanism. As shown in Figures S53–S57, the core-level spectra of both C 1s and Zn 2p of Zn-MOFs-1–5 are almost the same before and after UV light irradiation. However, the variation in those of the oxidants of O 1s and N 1s is discernible. The O 1s binding energy signal of Zn-MOFs-1–5 increases after UV irradiation compared to its pre-UV irradiation state. This elevation results from the dissociation of electrons from the ions on the O atoms. Conversely, Zn-MOFs-1–5 experience a noticeable shift toward a lower N 1s binding energy position after UV irradiation, as it receives electrons in this process. This further confirms that the electron transfer occurs between the O of carboxylate groups and the N of the pyridinium unit in Zn-MOFs-1–5. It is worth noting that Cl[−] also acts as an electron donor and participates in the electron transfer process in Zn-MOF-3. Despite the long distance of 4.61 Å from Cl[−] to N of the pyridinium unit exceeding the maximum electron transfer distance of 4 Å, some reported viologen-based complexes longer than that distance can facilitate electron transfer.^{41–43} Moreover, the photoluminescence of the H₄pdda ligand and viologen guests was investigated to understand the fluorescence emission mechanism of Zn-MOFs. The free H₄pdda

ligand showed weak photoluminescence emission at 394 nm, indicating that the fluorescence of Zn-MOF-0 could be attributed to the ligand-to-metal charge transition (LMCT) (Figures S57–S58). Additionally, the five viologen guests displayed photoluminescence emission bands at 486, 484, 517, 522, and 489 nm (Figures S57–S58). The luminescence emission of the compounds Zn-MOFs-1–5 can be attributed to the ligand-to-ligand charge transition (LLCT) and the presence of $\pi\cdots\pi$ stacking interactions between viologen guests and the host framework.^{44–49} Moreover, the principles of controlled modulation of fluorescent properties in this system were further investigated by determining the relationship between the emission of Zn-MOFs and the electron affinity (E_a) of the guest molecules (Table S6). As we all know, in the luminescent MOF-based charge-transfer system, luminescence emission is determined by the charge-transfer nature.^{30–52} Therefore, the wavelength signifies the energy gap between the exciplex's excited state and the ground state, primarily defined by the highest occupied molecular orbital (HOMO) of the donor and the lowest unoccupied molecular orbital (LUMO) of the acceptor. As the E_a of the guest corresponds to its LUMO energy level and the HOMO of H_4pdda remains similar in five hybrid compounds, a guest having a higher E_a value may generate an emission featuring a higher wavelength. For instance, the E_a values of $[dbbpy]^{2+}$ and $[debpy]^{2+}$ molecules are 8.5 and 8.8 eV, respectively, which are higher than the E_a values of other viologen guest molecules. Hence, Zn-MOF-4 and Zn-MOF-2 show higher emission wavelength (centered at 565.3 and 549.6 nm). Conversely, the $[bdbpy]^{2+}$ molecules possess minimum E_a values, and the compound Zn-MOF-5 has the lowest emission wavelength (centered at 491.9 nm). However, linear correlations could not be obtained between the emission maximums of the Zn-MOFs and the E_a values of the corresponding guests (Figure 7a). This is probably credited to the varying $\pi\cdots\pi$ interaction levels between the viologen guests and H_4pdda ligands (Figure 7b). In the previously reported luminescent MOFs or multicomponent crystal systems, the $\pi\cdots\pi$ interactions between the host and guest can affect the charge-transfer process, thereby impacting the luminescent properties of these compounds.^{53–56} In Zn-MOFs-2, 3, and 4, the varying degrees of $\pi\cdots\pi$ interactions between viologen molecules and H_4pdda ligands affect the respective Zn-MOFs emissions. Therefore, in these viologen-based host–guest compounds, both the E_a values of the viologen guests and the $\pi\cdots\pi$ interactions between the viologen guests and H_4pdda ligands determine fluorescence emissions. Besides, luminescence quenching could be attributed to the partial overlap between the emission bands of the initial sample and the absorption bands of the colored sample.

4. CONCLUSIONS

In summary, the five viologen-based host–guest materials were constructed with viologen as guests and 3D Zn-MOF as a host. These composite materials showed guest-dependent color-tunable emissions and photomodulated luminescence upon UV light radiation. Specifically, Zn-MOF-3 displayed excellent photochromism at intensities as low as $0.1 \mu\text{W}/\text{cm}^2$. This property was successfully applied in a readout UV colorimetric dosimeter. Zn-MOF-1 was used as a real-time sunlight sensor for personal UVA and UVB radiation doses. These MOFs showed fast recovery when kept in the dark for 5 h or heated at 50°C for 30 min, which is suitable for practical applications.

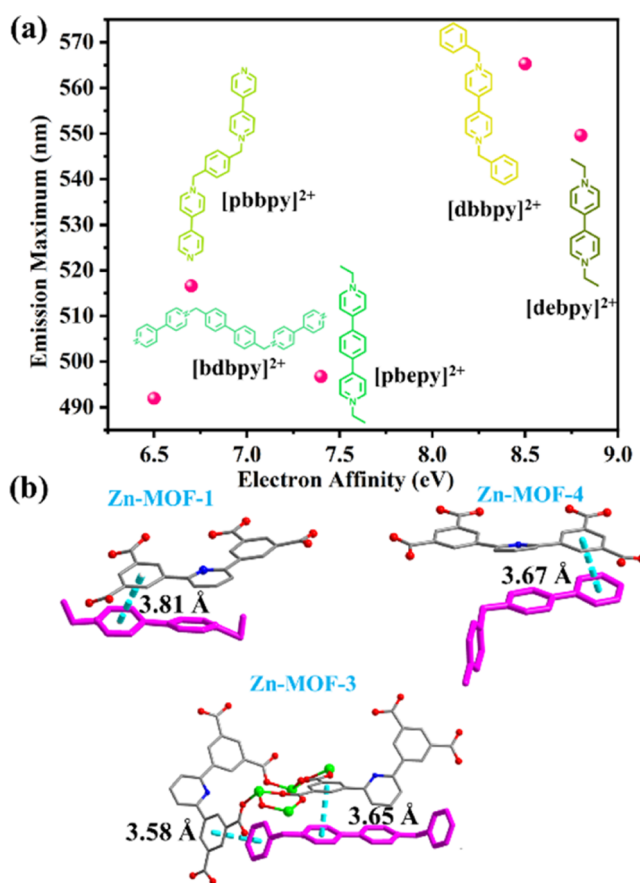


Figure 7. (a) Correlation between the emission maxima of Zn-MOFs-1–5 and E_a of guests. (b) $\pi\cdots\pi$ interactions between the guests and H_4pdda ligands.

The mechanisms of photochromism and photoluminescence modulation are also discussed. Successful syntheses of these host–guest compounds based on viologen are expected to encourage the discovery of other molecules for constructing host–guest composite materials for applications in photomodulated color switching and UV sensing.

■ ASSOCIATED CONTENT

Supporting Information

The Supporting Information is available free of charge at <https://pubs.acs.org/doi/10.1021/acsami.3c12012>.

Materials synthesis and characterization; FT-IR spectra; TGA analyses; experimental section; single-crystal X-ray diffraction; structural figures; XRD analyses; luminescence lifetimes and photoluminescence quantum yield analyses; photoluminescence and photochromism; ESR spectra; UV–vis spectra; XPS spectra analyses; DFT computation (PDF)

■ AUTHOR INFORMATION

Corresponding Author

Guannan Wang — School of Pharmacy, Shenyang Medical University, Shenyang 110034, China; orcid.org/0000-0003-3593-5589; Email: chemwanguannan@gmail.com

Authors

Haitao Han – College of Medical Engineering & the Key Laboratory for Medical Functional Nanomaterials, Jining Medical University, Jining 272067, China

Zheng Sun – College of Medical Engineering & the Key Laboratory for Medical Functional Nanomaterials, Jining Medical University, Jining 272067, China

Xia Zhao – College of Medical Engineering & the Key Laboratory for Medical Functional Nanomaterials, Jining Medical University, Jining 272067, China

Shujuan Yang – College of Medical Engineering & the Key Laboratory for Medical Functional Nanomaterials, Jining Medical University, Jining 272067, China

Complete contact information is available at:
<https://pubs.acs.org/10.1021/acsami.3c12012>

Notes

The authors declare no competing financial interest.

ACKNOWLEDGMENTS

We thank the Natural Science Foundation of Shandong Province (No. ZR2021QB163), the Higher Education Institutions' Youth Innovation Team of Shandong Province (600768002), and the Start-Up Grant of Jining Medical University (600910001).

REFERENCES

- (1) Ji, C. S.; Zhang, J.; Fan, R. Q.; Chen, Y. N.; Zhang, Y. F.; Sun, T. C.; Yang, Y. L. Lanthanide-MOFs based Host-guest Intelligent Dual-Stimulus Response Platform for Naked-eye and Ratiometric Fluorescent Monitoring of Food Freshness. *J. Mater. Chem. C* **2023**, *11*, 2514–2521.
- (2) Yam, V. W. W.; Chan, A. K. W.; Hong, E. Y. H. Charge-transfer processes in metal complexes enable luminescence and memory functions. *Nat. Rev. Chem.* **2020**, *4*, 528–541.
- (3) Hu, J. X.; Jiang, X. F.; Ma, Y. J.; Liu, X. R.; Ge, B. D.; Wang, A. N.; Wei, Q.; Wang, G. M. Optically actuating ultra-stable radicals in a large π -conjugated ligand constructed photochromic complex. *Sci. China Chem.* **2021**, *64*, 432–438, DOI: 10.1007/s11426-020-9891-4.
- (4) Yan, X.; Peng, H.; Xiang, Y.; Wang, J.; Yu, L.; Tao, Y.; Li, H. H.; Huang, W.; Chen, R. F. Recent Advances on Host–Guest Material Systems toward Organic Room Temperature Phosphorescence. *Small* **2022**, *18*, No. 2104073, DOI: 10.1002/smll.202104073.
- (5) Wang, Y. S.; Gao, H. Q.; Yang, J.; Fang, M. M.; Ding, D.; Tang, B. Z.; Li, Z. High Performance of Simple Organic Phosphorescence Host-Guest Materials and their Application in Time-Resolved Bioimaging. *Adv. Mater.* **2021**, *33*, No. 2007811.
- (6) Zhang, H. Y.; Wang, B. L.; Yu, X. W.; Li, J. Y.; Shang, J.; Yu, J. H. Carbon Dots in Porous Materials: Host-Guest Synergy for Enhanced Performance. *Angew. Chem., Int. Ed.* **2020**, *132*, 19558–19570.
- (7) Xie, L. S.; Skorupskii, G.; Dincă, M. Electrically Conductive Metal-Organic Frameworks. *Chem. Rev.* **2020**, *120*, 8536–8580.
- (8) Zhang, X.; Chen, Z.; Liu, X. Y.; Hanna, S. L.; Wang, X. J.; Ledari, R.; Maleki, A.; Li, P.; Farha, O. K. A historical overview of the activation and porosity of metal–organic frameworks. *Chem. Soc. Rev.* **2020**, *49*, 7406–7427, DOI: 10.1039/d0cs00997k.
- (9) Dutta, A.; Pan, Y.; Liu, J. Q.; Kumar, A. Multicomponent isorecticular metal-organic frameworks: Principles, current status and challenges. *Coord. Chem. Rev.* **2021**, *445*, No. 214074.
- (10) Wang, T.; Zhang, L.; Liu, J.; Li, X. X.; Yuan, L.; Li, S. L.; Lan, Y. Q. A viologen-functionalized metal–organic framework for efficient CO₂ photoreduction reaction. *Chem. Commun.* **2022**, *58*, 7507–7510.
- (11) Rice, A. M.; Martin, C. R.; Galitskiy, V. A.; Berseneva, A. A.; Leith, G. A.; Shustova, N. B. Photophysics Modulation in Photo-switchable Metal-Organic Frameworks. *Chem. Rev.* **2020**, *120*, 8790–8813, DOI: 10.1021/acs.chemrev.9b00350.
- (12) Li, X.; Zhang, S.; Zhang, L.; Yang, Y.; Zhang, K.; Cai, Y. C. Viologen-Based Cationic Metal-Organic Framework for Antibiotics Detection and MnO₄[−] Removal in Water. *Cryst. Growth Des.* **2022**, *22*, 3991–3997, DOI: 10.1021/acs.cgd.2c00170.
- (13) Guo, B. B.; Yin, J. C.; Li, N.; Fu, Z. X.; Han, X.; Xu, J. L.; Bu, X. H. Recent Progress in Luminous Particle-Encapsulated Host-Guest Metal-Organic Frameworks for Optical Applications. *Adv. Opt. Mater.* **2021**, *9*, No. 2100283.
- (14) Lin, Y. S.; Su, P. C.; Li, W. B. Chemical vapor deposition of guest-host dual metal-organic framework heterosystems for high-performance mixed matrix membranes. *Appl. Mater. Today* **2022**, *27*, No. 101462.
- (15) Li, F. P.; Li, J. Q.; Wang, K.; Ao, M.; Qiu, J. S.; Zhang, X. W.; Wang, H.; Pham, G. H.; Liu, S. M. Co/Co₆Mo₆C@C nanoreactors derived from ZIF-67 composite for higher alcohols synthesis. *Composites, Part B* **2021**, *209*, No. 108608.
- (16) Li, Y. Y.; Zhou, B. X.; Zhang, H. W.; Huang, T.; Wang, Y. M.; Huang, W. Q.; Hu, W. Y.; Pan, A. L.; Fan, X. X.; Huang, G. F. A host–guest self-assembly strategy to enhance π -electron densities in ultrathin porous carbon nitride nanocages toward highly efficient hydrogen evolution. *Chem. Eng. J.* **2022**, *430*, No. 132880.
- (17) Gutiérrez, M.; Zhang, Y.; Tan, J. C. Confinement of Luminescent Guests in Metal-Organic Frameworks: Understanding Pathways from Synthesis and Multimodal Characterization to Potential Applications of LG@MOF Systems. *Chem. Rev.* **2022**, *122*, 10438–10483.
- (18) Dsouza, R. N.; Pischel, U.; Nau, W. M. Fluorescent Dyes and Their Supramolecular Host/Guest Complexes with Macrocycles in Aqueous Solution. *Chem. Rev.* **2011**, *111*, 7941–7980.
- (19) Li, M. L.; Ren, G. J.; Yang, W. T.; Yang, Y. H.; Yang, W. K.; Gao, Y.; Qiu, P. F.; Pan, Q. H. Dual-emitting piezofluorochromic dye@MOF for white-light generation. *Chem. Commun.* **2021**, *57*, 1340–1343.
- (20) Zhang, D. S.; Gao, Q.; Zhang, Z.; Liu, X. T.; Zhao, B.; Xuan, Z. H.; Hu, T. L.; Zhang, Y. H.; Zhu, J.; Bu, X. H. Rational Construction of Highly Tunable Donor-Acceptor Materials Based on a Crystalline Host-Guest Platform. *Adv. Mater.* **2018**, *30*, No. 1804715.
- (21) Liu, X. Y.; Xing, K.; Li, Y.; Tsung, C. K.; Li, J. Three Models to Encapsulate Multicomponent Dyes into Nanocrystal Pores: A New Strategy for Generating High-Quality White Light. *J. Am. Chem. Soc.* **2019**, *141*, 14807–14813.
- (22) Han, S. D.; Hu, J. X.; Wang, G. M. Recent advances in crystalline hybrid photochromic materials driven by electron transfer. *Coord. Chem. Rev.* **2022**, *452*, No. 214304.
- (23) Zhao, G. Z.; Liu, W. Y.; Yuan, F.; Liu, J. J. Two host-guest 2D MOFs based on hexyl viologen cations: Photochromism. *Dyes Pigm.* **2021**, *188*, No. 109196.
- (24) Yu, L. M.; Fu, J. J.; Xia, S. B.; Liu, J. J. Encapsulating viologen derivatives in anionic MOFs: Photochromism and photocontrolled luminescence. *J. Solid. State Chem.* **2022**, *305*, No. 122616.
- (25) Hu, S. Z.; Zhang, J.; Chen, S. H.; Dai, J. C.; Fu, Z. Y. Efficient Ultraviolet Light Detector Based on a Crystalline Viologen-Based Metal-Organic Framework with Rapid Visible Color Change under Irradiation. *ACS Appl. Mater. Interfaces* **2017**, *9*, 39926–39929.
- (26) Li, L.; Tu, Z. M.; Hua, Y.; Li, X. N.; Wang, H. Y.; Zhang, H. A novel multifunction photochromic metal-organic framework for rapid ultraviolet light detection, amine-selective sensing and inkless and erasable prints. *Inorg. Chem. Front.* **2019**, *6*, 3077–3082.
- (27) Liu, J. F.; Shi, X. L.; Qu, Y. C.; Wang, G. N. Functionalized ZnMnFe₂O₄-PEG-FA nanoenzymes integrating diagnosis and therapy for targeting hepatic carcinoma guided by multi-modality imaging. *Nanoscale* **2023**, *15*, 11013–11025.
- (28) Zhang, D. S.; Gao, Q.; Chang, Z.; Liu, X. T.; Zhao, B.; Xuan, Z. H.; Hu, T. L.; Zhang, Y. H.; Zhu, J.; Bu, X. H. Rational Construction of Highly Tunable Donor-Acceptor Materials Based on a Crystalline Host-Guest Platform. *Adv. Mater.* **2018**, *30*, No. 1804715.
- (29) Takashima, Y.; Martinez, V. M.; Furukawa, S.; Kondo, M.; Shimomura, S.; Uehara, H.; Nakahama, M.; Sugimoto, K.; Kitagawa,

S. Molecular decoding using luminescence from an entangled porous framework. *Nat. Commun.* **2011**, *2*, No. 168.

(30) Ono, T.; Sugimoto, M.; Hisaeda, Y. Multicomponent Molecular Puzzles for Photofunction Design: Emission Color Variation in Lewis Acid-Base Pair Crystals Coupled with Guest-to-Host Charge Transfer Excitation. *J. Am. Chem. Soc.* **2015**, *137*, 9519–9522.

(31) He, X. L.; Zhou, J.; Wang, W. B.; Xuan, W. P.; Yang, X.; Jin, H.; Luo, J. K. High performance dual-wave mode flexible surface acoustic wave resonators for UV light sensing. *J. Micromech. Microeng.* **2014**, *24*, No. 055014.

(32) Li, L.; Zou, Y. C.; Hua, Y.; Li, X. N.; Wang, Z. H.; Zhang, H. Polyoxometalate-viologen photochromic hybrids for rapid solar ultraviolet light detection, photoluminescence-based UV probing and inkless and erasable printing. *Dalton Trans.* **2020**, *49*, 89–94.

(33) Wu, J. B.; Lou, L. Q.; Han, Y. D.; Xu, Y.; Zhang, X.; Wang, Z. P. Ionothermal synthesis of a photochromic inorganic-organic complex for colorimetric and portable UV index indication and UVB detection. *RSC Adv.* **2020**, *10*, 41720–41726.

(34) Wang, M. L.; Wei, T. W.; Jiang, L.; Wang, J.; Li, Y.; Wu, W. Y.; Huang, X. J.; Wang, F.; Lu, S.; Chen, X. Q. A naphthalimide-based fluorescent probe for quantitative sensing of UV light. *Dyes Pigm.* **2022**, *206*, No. 110673.

(35) Kurz, W.; Yetisen, A. K.; Kaito, M. V.; Fuchter, M. J.; Jakobi, M.; Elsner, M.; Koch, A. W. UV-Sensitive Wearable Devices for Colorimetric Monitoring of UV Exposure. *Adv. Opt. Mater.* **2020**, *8*, No. 1901969.

(36) Zou, W. Y.; González, A.; Jampaiah, D.; Ramanathan, R.; Taha, M.; Walia, S.; Sriram, S.; Bhaskaran, M.; Vera, J. M. D.; Bansal, V. Skin color-specific and spectrally-selective naked-eye dosimetry of UVA, B and C radiations. *Nat. Commun.* **2018**, *9*, No. 3743.

(37) Liu, J. J. Multi-responsive host-guest MOFs derived from ethyl viologen cations. *Dyes Pigm.* **2019**, *163*, 496–501, DOI: 10.1016/j.dyepig.2018.12.033.

(38) Hao, P. F.; Liu, X.; Guo, C. Y.; Zhao, G. Z.; Li, G. P.; Shen, J. J.; Fu, Y. L. Lattice solvent controlled photochromism of tripyridyl-triazine-based zinc bromide complexes. *Inorg. Chem. Front.* **2022**, *9*, 879–888.

(39) Li, M. H.; You, M. H.; Lin, M. J. Photochromism- and Photoluminescence-Tunable Heterobimetallic Supramolecular Hybrid Isomers. *Cryst. Growth Des.* **2021**, *21*, 2856–2867.

(40) Liu, J. J.; Que, Q. T.; Liu, D.; Suo, H. B.; Liu, J. M.; Xia, S. B. A multifunctional photochromic metal-organic framework with Lewis acid sites for selective amine and anion sensing. *CrystEngComm* **2020**, *22*, 4124–4129.

(41) Chen, C.; Sun, J. K.; Zhang, Y. J.; Yang, X. D.; Zhang, J. Flexible Viologen-Based Porous Framework Showing X-ray Induced Photochromism with Single-Crystal-to-Single-Crystal Transformation. *Angew. Chem., Int. Ed.* **2017**, *56*, 14458–14462.

(42) Liu, J.; Lu, Y.; Li, J.; Lu, W. UV and X-ray dual photochromic properties of three CPs based on a new viologen ligand. *Dyes Pigm.* **2020**, *177*, No. 108276.

(43) Wu, J. B.; Tao, C. Y.; Li, Y.; Yan, Y.; Li, J. Y.; Yu, J. H. Methylviologen-templated layered bimetal phosphate: a multifunctional X-ray-induced photochromic material. *Chem. Sci.* **2014**, *5*, 4237–4241.

(44) Cui, Y. J.; Yue, Y. F.; Qian, G. D.; Chen, B. L. Luminescent Functional Metal-Organic Frameworks. *Chem. Rev.* **2012**, *112*, 1126–1162.

(45) Li, X.; Wang, X. W.; Zhang, Y. H. Blue photoluminescent 3D Zn(II) metal-organic framework constructing from pyridine-2,4,6-tricarboxylate. *Inorg. Chem. Commun.* **2008**, *11*, 832–834.

(46) Elleuch, S.; Triki, I.; Abid, Y. Optical and charge transfer properties of a new cadmium based metal-organic-framework material. *Mater. Res. Bull.* **2022**, *150*, No. 111754.

(47) Zheng, Q. S.; Yang, F. L.; Deng, M. L.; Ling, Y.; Liu, X. F.; Chen, Z. X.; Wang, Y. H.; Weng, L. H.; Zhou, Y. M. A Porous Metal-Organic Framework Constructed from Carboxylate-Pyrazolate Shared Heptanuclear Zinc Clusters: Synthesis, Gas Adsorption, and Guest-

Dependent Luminescent Properties. *Inorg. Chem.* **2013**, *52*, 10368–10374.

(48) Hou, L.; Lin, Y. Y.; Chen, X. M. Porous Metal-Organic Framework Based on μ_4 -oxo Tetrazinc Clusters: Sorption and Guest-Dependent Luminescent Properties. *Inorg. Chem.* **2008**, *47*, 1346–1351.

(49) Lee, E. Y.; Jang, S. Y.; Suh, M. P. Multifunctionality and Crystal Dynamics of a Highly Stable, Porous Metal-Organic Framework [Zn₄O(NTB)₂]. *J. Am. Chem. Soc.* **2005**, *127*, 6374–6381.

(50) Kulkarni, C.; Periyasamy, G.; Balasubramanian, S.; George, S. J. Charge-transfer complexation between naphthalene diimides and aromatic solvents. *Phys. Chem. Chem., Phys.* **2014**, *16*, 14661–14664.

(51) Sun, J. K.; Chen, C.; Cai, L. X.; Ren, C. X.; Tan, B.; Zhang, J. Mechanical grinding of a single-crystalline metal-organic framework triggered emission with tunable violet-to-orange luminescence. *Chem. Commun.* **2014**, *50*, 15956–15959.

(52) Yang, D. D.; Meng, F. Q.; Zheng, H. W.; Shi, Y. S.; Xiao, T.; Jin, B.; Liang, Q. F.; Zheng, X. J.; Tan, H. W. Two multifunctional stimuli-responsive materials with room-temperature phosphorescence and their application in multiple dynamic encryption. *Mater. Chem. Front.* **2022**, *6*, 2709–2717.

(53) Li, R.; Wang, S. H.; Liu, Z. F.; Chen, X. X.; Xiao, Y.; Zheng, F. K.; Guo, G. C. An Azole-Based Metal-Organic Framework toward Direct White-Light Emissions by the Synergism of Ligand-Centered Charge Transfer and Interligand π - π Interactions. *Cryst. Growth Des.* **2016**, *16*, 3969–3975.

(54) Ding, Z. Y.; Shang, H. X.; Zhang, S. T.; Han, W. K.; Li, B.; Jiang, S. M. Insight from Molecular Packing: Charge Transfer and Emission Modulation through Cocrystal Strategies. *Cryst. Growth Des.* **2020**, *20*, 5203–5210.

(55) Jiang, W.; Ma, X. Y.; Liu, D.; Zhao, G. M.; Tian, W. W.; Sun, Y. M. Modulation of charge transfer and π - π interaction toward tunable fluorescence emission in binary cocrystals composed of carbazole derivatives and 1,2,4,5-tetracyanobenzene. *Dyes Pigm.* **2021**, *193*, No. 109519.

(56) Fan, J. Z.; Zhang, Y. C.; Ma, Y. Y.; Song, Y. Z.; Lin, L. L.; Xu, Y. Y.; Wang, C. K. The role of intermolecular interactions in regulating the thermally activated delayed fluorescence and charge transfer properties: a theoretical perspective. *J. Mater. Chem. C* **2020**, *8*, 8601–8612.